A Method to Reject Random Coincidences and Extract True from Multiple Coincidences in PET using 3-D Detectors

Garry Chinn and Craig S. Levin, *Member, IEEE*

***Abstract*–In this work, we develop a new method to reject random coincidences and identify true coincidences from multiple photon coincidences using 3-D photon positioning PET detectors. We are developing scintillation and cadmium zinc telluride (CZT) detectors with the ability to position the 3-D coordinates of every detector interaction with 1 mm intrinsic spatial and <2.5% FWHM energy resolution at 511 keV. For multiple interactions, the position of the first two interactions and the energy of the first interaction are used to electronically collimate single photons by the kinematics of Compton scatter. We use a "direction window" to determine coincident lines of response. Using a hypothesis testing framework, we derive a direction window threshold that maximizes the noise equivalent counts (NEC) of the system. This new method is compared against conventional coincidence processing for a dual-panel breast CZT PET system under development in our laboratory. For a simplified approximation of our maximum NEC derivation, we show that the addition of a direction window reduced random coincidences by 55-60%. At high activities, the ability to recover trues from multiple coincidences increased the true coincidence rate of the system by as much as 11%.**

I. Introduction

CADMIUM zinc telluride (CZT) can be used to build three-dimensional (3-D) PET detectors with high spatial and energy resolutions [1], [2]. The disadvantages of CZT include relatively poor time resolution [2], [4], [5] and low photoelectric fraction compared to inorganic scintillator crystals coupled to photomultiplier and semiconductor photodetectors. In PET, good time resolution is important because coincidence detection [6] is used to determine the lines of response (LOR). Poor time resolution can reduce the effectiveness of coincidence detection by increasing the rate of multiple coincidences and random coincidences. Multiple coincidences occur when more than two photon events are recorded in the time window. In this case, the true photon pair cannot be determined and the photons are discarded, reducing the sensitivity of the system. Random coincidence events occur when two photons detected in the coincidence time window are from unrelated positron-electron annihilation events. Random coincidences reduce the reconstructed image contrast.

Manuscript received November 4, 2008. This work was supported in part by the NIH (NIH R01 CA119056, NIH R33 EB003283, and NIH R01 CA120474).

G. Chinn and C. S. Levin are with the Dept. of Radiology and Molecular Imaging Program at Stanford University, Stanford CA. USA (corresponding author: G. Chinn, phone: 650-736-7248; fax: 650-724-1499; e-mail: gchinn@stanford.edu and cslevin@stanford.edu).

For 3-D detectors with excellent spatial and energy resolution, the kinematics of Compton scatter in the detector can be used to electronically collimate photons [7], [8], [9], [10]. In this work, we use Compton kinematics to estimate the direction of the detected photons in order to differentiate true coincidences from random coincidences. This method improves the rejection of random and multiple coincidences to be used for reconstruction. We develop a likelihood ratio test that maximizes the noise equivalent counts (NEC) of the system. We provide Monte Carlo simulation results comparing this new approach against conventional coincidence detection.

II. Background

A. CZT Detectors

CZT is a wide bandgap, room temperature semiconductor that may be used for direct detection of 511 keV photons. In our design shown in Fig. 1, anode and cathode cross strips sample the interaction position along two dimensions. The position in the third dimension is computed from the cathode-to-anode signal ratio. A 1 mm x 1 mm x 1 mm spatial resolution can be achieved by using 1 mm pitch orthogonal anode and cathode strips. The energy resolution has been measured at ≤2.5% FWHM for 511 keV photons [1]. These CZT detectors are then stacked in an edge-on configuration to provide high intrinsic detection efficiency. With a minimum photon traversal distance of 4 cm, the single (coincidence) 511 keV photon detection efficiency is 86% (74%).

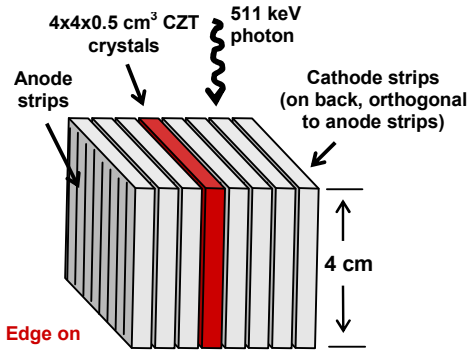

Fig. 1. The 3-D CZT detector with orthogonal cross-strip anodes and cathodes is shown. The detector is oriented edge-on to facilitate high intrinsic photon detection efficiency owing to >99% crystal packing fraction and a minimum photon traversal path of 4 cm. With 1 mm pitch anode and cathode strips, the detector achieves 1 mm³ spatial resolution with an energy resolution of 2.5% FWHM for 511 keV photons [1].

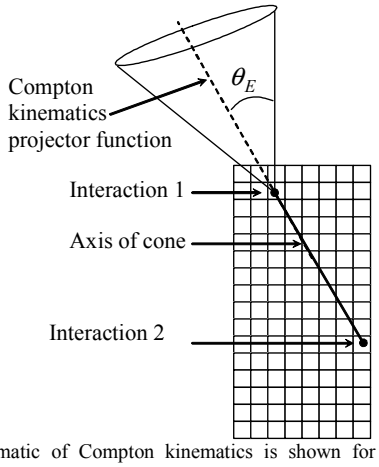

Fig. 2. A schematic of Compton kinematics is shown for the 3-D CZT detector. The spatial location of two interactions in the detector determines the axis of the cone. The measured energies of the interactions determines the angle of the cone.

B. Electronic Collimation by Compton Kinematics

With high 3-D spatial and energy resolution along with the capability to position individual Compton interactions in the detector, the kinematics of Compton scatter in the detector can be used to electronically collimate photons [7], [8], [9], [10]. Fig. 2 illustrates the process of *Compton collimation*. For 3-D PET detectors, Compton collimation can only be performed when the position and energy of the first two interactions in the detector are measured. Monte Carlo simulations with GATE (GEANT4) [11] suggest that 77% of all detected single photon events involve one or more Compton interactions in the detectors. A cone-surface projector function is then formed for the single photon event where the line formed by the two interactions form the cone axis and the cone half angle θ_E is calculated by

$$\cos\theta_E = 1 - m_e c^2 \left(\frac{1}{E_1} - \frac{1}{E_0} \right) \tag{1}$$

where E_0 is the incident photon energy and E_1 is the photon energy after the first Compton interaction deposits energy e_1 in the detector, m_e is the mass of an electron, and c is the speed of light. Doppler broadening, energy blurring, and spatial blurring in the 3-D detector leads to angular blurring of the cone half-angle θ_E [12].

C. Clustering and Sequencing Interactions

In order to perform Compton collimation, the detector interactions must first be grouped into photons and sequenced. Compton interactions tend to be forward scattering and given the stopping power of CZT, the interactions for a single photon will generally be in close proximity. The clustering problem becomes more difficult when interactions from multiple photon events occur in the same or adjacent detectors. However, the frequency in which multiple photons are detected in close proximity is low and clustering errors can be considered a 2nd order effect.

Various studies have investigated the sequencing of interactions in three-dimensional detectors [13]. For the energy and spatial resolution of CZT detectors, high sequencing accuracy has been shown to be obtainable. Pratx and Levin [13] showed that 77-78% sequencing accuracy for two and three interactions was achievable for CZT detectors with 3% energy resolution and 1 mm by 1 mm by 1 mm spatial resolution.

In this work, it is assumed that the detector interactions have been accurately clustered and sequenced.

III. Direction Window Classifier

In this section, we derive a *maximum NEC* (noise equivalent counts) *direction window classifier*. The classifier uses measurements of interaction time, energy, and position from 3-D PET detectors to identify true coincidences from random coincidences.

A. Energy Window

The maximum NEC direction window is used in combination with the conventional energy window and time window. An energy window is used to reduce the acceptance rate of photons that scattered in tissue. If the total photon energy is outside the 511 keV photopeak window, it is rejected as a photon that has undergone Compton scattering within tissue.

B. Time Window

A *time window* is applied to create a set of photons called the *time neighborhood (set)* for each photon. For a time window of duration τ, the number of photons in one time neighborhood k will be a Poisson distributed random number. Let H_T denote the hypothesis that a pair of detected photons were a true positron-electron annihilation pair. The average number of trues in a time neighborhood with k photons is given by

$$P(H_T \mid k) = E[k_T \mid k] / Q(k)$$
$$= \frac{\sum_{n=0}^{Q(k)} P[N(\tau) = n \mid \lambda_c] P[N(\tau) = k - 2n \mid \lambda_s - 2\lambda_c] n}{Q(k) \sum_{n=0}^{Q(k)} P[N(\tau) = n \mid \lambda_c] P[N(\tau) = k - 2n \mid \lambda_s - 2\lambda_c]} \tag{2}$$

where λ_c (true coincidence rate) is the rate that both annihilation photons appear in the time neighborhood set, λ_s is the windowed singles rate, and the Poisson probability mass function is

$$P[N(\tau) = k \mid \lambda] = \frac{e^{-\lambda\tau} (\lambda\tau)^k}{k!} \tag{3}$$

since the half-life $>> \tau$. The maximum number of trues in the time window is given by

$$Q(k) = \begin{cases} k/2 & \text{if } k \text{ even} \\ (k-1)/2 & \text{if } k \text{ odd} \end{cases} \tag{4}$$

In (2), the term $P[N(\tau) = n \mid \lambda_c]$ denotes the probability that there are n annihilation pairs in the coincidence window and $P[N(\tau) = k - 2n \mid \lambda_s - 2\lambda_c]$ is the probability that the

remaining $k - 2n$ photons are singles from different annihilation events.

C. Direction Window

After energy and time windowing, a *direction window* (DW) is applied to identify true coincidences. Compton kinematics is used to estimate the direction of the incident photon. The line defined by the first two interactions will be referred to as the Compton cone axis and is shown as a large black dotted line in Fig. 3. The calculated Compton scattering angle θ_E as determined by the measured energy of the first interaction using (1) and represents the direction of the incident photon relative to the Compton cone axis. Given any pair of detected photons, a LOR can be determined as the line through the detected positions. The angle between the correct LOR and the Compton cone axis is denoted by θ_P. The difference between these angles $\theta = |\theta_E - \theta_P|$ is a random variable, which will be called the *direction difference angle*. If the LOR is the result from true coincidences, we assume the distribution is approximately Gaussian distributed

$$p_{H_T}(\theta) = \frac{2(2.3548)}{F(2\pi)^{1/2}} e^{-2.773\theta^2/F^2} + \mathrm{erfc}(2.3548\pi/\sqrt{2}F) \qquad (5)$$

where F is the full-width at half-maximum of the angular resolution of the detector. The angular resolution is dependent on the energy resolution, spatial resolution, and detector geometry. If the LOR is the result of two photons from different annihilation events (random coincidence hypothesis denoted by H_R), the distribution is approximately uniformly distributed where

$$p_{H_R}(\theta) = \frac{1}{\pi} \qquad (6)$$

For k photons in the time neighborhood set, let the angle θ_i correspond to the direction difference angle for photon m and n_i, where $i = 1 \ldots k-1$ and with $L_i = (m, n_i)$ specifying the LOR between the two photons. There are k possible hypotheses for photon m: photon m and n_i are a true coincidence or photon m is a single photon. A likelihood ratio [16] is used to test each hypothesis. Hypothesis H_i corresponds to photon m and n_i forming a true coincidence

$$D = H_i : \begin{cases} \dfrac{p_{H_T}(\theta_i)}{p_{H_R}(\theta_i)} \geq \dfrac{P(H_R)}{P(H_T)} \text{ and} \\ \dfrac{p_{H_T}(\theta_i)}{p_{H_T}(\theta_j)} \geq \dfrac{P(H_j \mid \theta_{E,j}, \theta_{P,j})}{P(H_i \mid \theta_{E,i}, \theta_{P,i})} \end{cases} \qquad (7)$$

where $i, j = 1 \ldots k-1, \forall i \neq j$.

We may simplify the decision rule by assuming that the *a priori* probabilities $P(H_i \mid \theta_{E,i}, \theta_{P,i})$ are equal for all θ_i. If $\theta_i \geq \theta_0$ for $i = 1 \ldots k-1$, H_s is the hypothesis that photon m is a single photon. Because every photon n_i may have a different time neighborhood set from photon m, the time neighborhood sets of each photon n_i are also tested. Substituting (5) into the lower part of (7) yields

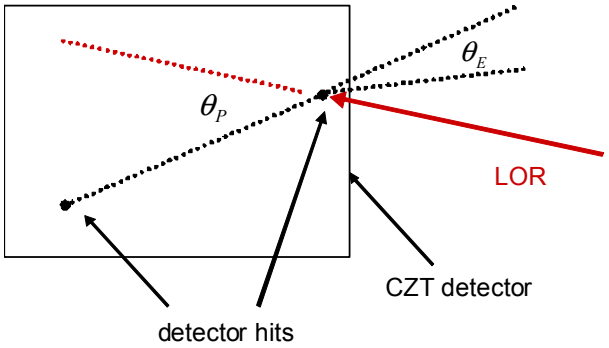

Fig. 3. Compton kinematics is used to calculate the expected angle between the LOR and the first two interactions in the detector. The large black dotted line formed by the first two interactions is the Compton cone axis.

$$\log\frac{2.3548}{(2\pi)^{1/2}F_i} - 2.773\theta_i^2/F_i \geq \log\frac{2.3548}{(2\pi)^{1/2}F_j} - 2.773\theta_j^2/F_j$$

$$\theta_i^2 \leq \frac{F_i}{F_j}\theta_j^2 + \frac{1}{2.773}\left(\log\frac{2.3548}{(2\pi)^{1/2}F_i} - \log\frac{2.5348}{(2\pi)^{1/2}F_j}\right).$$

Substituting (5) and (6) into the top of (7) and assuming that $F_i \cong F_j$, the decision rule of (7) simplifies to

$$D = H_i : \theta_i < \theta_0, \theta_i < \theta_j, \text{ and } \theta_i < \theta_{j,j'} \qquad (8)$$

for every $j \neq i$ and for all j' in the time neighborhood of j where θ_0 is some the direction window threshold.

D. NEC Objective Function

In this work, the direction window thresholds are chosen to maximize the noise equivalent counts (NEC) [17]

$$\theta_0 = \arg\max\left(\frac{T^2}{T+S+R}\right) \qquad (9)$$

where T is the number of trues (correctly identified annihilation pairs), R is the number of random pairs, and S is the number of scattered annihilation pairs. The NEC is an estimate of the detector signal-to-noise ratio.

The true rate can be expressed as a function of the decision probability

$$T = E\left[P(H_T)P(D_i \mid H_i)\right]. \qquad (10)$$

The expected number of randoms can be expressed as

$$R = E\left[P(H_T)P(D_i \mid H_j) + (1 - P(H_T))P(D_T \mid H_R)\right], \qquad (11)$$

which simplifies to

$$R = E\left[P(H_T)P(D_i \mid H_j) + (1 - P(H_T))(1 - P(D_R \mid H_R))\right]. \qquad (12)$$

The decision probabilities are calculated using (2)-(8). Let D_i and H_i denote the decision and the hypothesis that the i-th pair is a true coincidence, respectively. Also, let the vector $\boldsymbol{\theta} = \theta_1 \ldots \theta_{k-1}$. Then the probability that the classifier correctly identifies the i-th true is

$$P(D_i \mid H_i, \theta_0) = \prod_{j \neq i} P(\theta_i < \theta_j \mid H_i)\, P(R_i \mid H_i) \qquad (13)$$

where the region $R_i = \{\theta_i < \theta_0\}$ and $\theta_i = \min_{j=1\ldots k} \{\theta_j\}$, so that

$$P(D_i \mid H_i, \theta_0) = P(\theta_i < \theta_{j=1\ldots k-1, j\neq i} \mid H_i) \int_{\theta \le \theta_o} p_{H_T}(\theta) d\theta = \left(1 - \int_{\theta \le \theta_i} p_{H_R}(\theta) d\theta\right)^{k-2} \int_{\theta \le \theta_o} p_{H_T}(\theta) d\theta$$

Because the erfc term from (5) is small, it is assumed to be zero, resulting in

$$P(D_i \mid H_i, \theta_0) = (1 - \theta_i / \pi)^{k-2} \operatorname{erf}(2.3548\theta_0 / \sqrt{2}F) \quad (14)$$

The probability of classifying the photons as a random in the case of a random is

$$P(D_R \mid H_R, \theta_0) = \prod_i P(R_i^C \mid H_R) = \left(1 - \int_{\theta \le \theta_0} p_{H_R}(\theta) d\theta\right)^{k-1}$$

yielding

$$P(D_R \mid H_R, \theta_0) = (1 - \theta_0 / \pi)^{k-1}. \quad (15)$$

Similarly, it can be shown that the probability of choosing to pair with photon *i* when pairing with photon *j* forms a true coincidence is

$$P(D_i \mid H_j) = \left(1 - (1 - \theta_0 / \pi)^{k-2}\right)\left(1 - \operatorname{erf}(2.3548\theta_i / \sqrt{2}F)\right) \quad (16)$$

Using (10)-(14), the true rate is

$$T(\boldsymbol{\theta}) = P(H_T \mid k)(1 - \theta_i / \pi)^{k-2} \operatorname{erf}(2.3548\theta_0 / \sqrt{2}F) \quad (17)$$

and the random rate is

$$R(\boldsymbol{\theta}) = P(H_T \mid k)\left[1 - (1 - \theta_0 / \pi)^{k-2}\left(1 - \operatorname{erf}\left(\frac{2.3548\theta_i}{\sqrt{2}F}\right)\right) + \left[1 - P(H_T \mid k)\right]\left[1 - (1 - \theta_0 / \pi)^{k-1}\right]\right] \quad (18)$$

Because these rates are a function of the number of photons in the time neighborhood, the direction window threshold will also vary depending on the number of photons in each time neighborhood. Exhaustive search could be used since the objective is to find the direction window threshold θ_0 that maximizes NEC over the interval [0,π]. To perform this search we use a gradient ascent approach, where the gradient of the NEC as a function of the angular threshold θ_0 is given by

$$\frac{d}{d\theta_0}\mathrm{NEC} = \frac{2T(T+S+R)\frac{dT}{d\theta_0} - T^2\left(\frac{dT}{d\theta_0} + \frac{dR}{d\theta_0}\right)}{(T+S+R)^2} \quad (19)$$

where

$$\frac{d}{d\theta_0}T = \frac{2.3548\sqrt{2}}{\sqrt{\pi}F} P(H_T)(1 - \theta_i / \pi)^{k-2} e^{-\frac{2.3548\theta_0^2}{F^2}} \quad (20)$$

$$\frac{dR}{d\theta_0} = P(H_T \mid k)\left(1 - \operatorname{erf}\left(\frac{2.3548\theta_i}{\sqrt{2}F}\right)\right)\frac{k-2}{\pi}(1 - \theta_0 / \pi)^{k-3} + \left[1 - P(H_T \mid k)\right]\frac{(k-1)}{\pi}(1 - \theta_0 / \pi)^{k-2} \quad (21)$$

The PDF of the direction difference angle for tissue scattered photons will be modeled by Monte Carlo simulations. Here a uniform distribution was first studied to simplify the formulation.

E. Trues and Singles Rate Estimation

The *a priori* trues rate and singles rate for each detector and LOR bin need to be estimated. The singles rate was estimated by Monte Carlo simulation. Monte Carlo simulations using *a priori* digital phantoms were used to provide an initial estimate of the trues rates. The decision thresholds θ_0 calculated from these initial rates were then used to reconstruct an image.

IV. METHODS

A dual-panel CZT PET system for breast imaging was simulated using GRAY [18]. A schematic of the system is shown in Fig. 4. The activity from the body is shielded by 5 mm of tungsten surrounding the detectors. The breasts were compressed to 6 cm. The detectors were simulated with a 1 mm x 1 mm x 1 mm spatial resolution. The energy blur was simulated as Gaussian random noise sources with FWHM

$$\Delta e = \sqrt{6^2 + (0.022e)^2} \quad (25)$$

where *e* is the energy of the interaction in keV. This assumes that the readout electronics contributes a 6 keV FWHM white Gaussian noise source.

The angular resolution for Compton collimation was modeled by a simple numerical simulation. To model angular resolution vs. E_1, the Compton scattering angle was calculated using (1) with E_1 varying from 170 keV to 490 keV in increments of 20 keV with noise added according to (25). A Gaussian curve was fitted to the angular distribution produced from 100,000 trials. The angular resolution vs. the distance between the first two interactions was also determined using a simple numerical model. The length of a line segment was varied from 1 mm to 30 mm in increments of 1 mm with 1 mm FWHM 3-D Gaussian noise added to each endpoint of the segment. A Gaussian curve was fitted to the distribution of the angular orientation of the line segment produced from 100,000 trials. To calculate *F*, first described in (5), these two angular resolution components were added in quadrature.

A digital human phantom was used in this study as shown in Fig. 4. The phantom consists of uniform activity in the body, activity in the heart and spherical lesions in the breast ranging in size from 1 mm to 1.75 mm.

We compared different methods for identifying LOR counts. For these cases, we used an 8 ns time window (assuming 8 ns FWHM coincidence time resolution [1]):

1. **Standard coincidence method**: When exactly two photons were detected within the energy and time window, a LOR count was recorded for the detected positions.
2. **The direction window with a fixed threshold chosen to maximize the NEC for each data set**: This approach was used to verify that the proposed algorithm is correctly maximizing the NEC. By trial and error, a global DW

threshold was adjusted until the maximum NEC was realized for each data set.

3. **The direction window using the proposed algorithm**: The DW threshold was calculated by maximizing (9) with the trues and random rates given by (15) and (16).

Images were reconstructed using an ordered subset list-mode maximum likelihood expectation maximization (OS ML-EM) algorithm [19], [20], [21].

V. Results

In Table 1, the NEC for the standard coincidence method using only energy and coincidence time windows was compared against the NEC of the optimal fixed DW threshold and the proposed maximum NEC DW algorithm. The breast of the digital human phantom (Fig. 4) with 50:1 sphere to background activity was scanned for 5 seconds. Five scans were performed with 1, 5, 10, 20, and 30 mCi of total activity in the phantom. ~10 mCi total activity is the most clinically relevant scanned activity. For the optimized fixed DW, a fixed DW was chosen by trial and error to maximize the NEC. The DW threshold in radians used for each case is shown in parenthesis. The maximum NEC algorithm uses a DW threshold that varies with the angular resolution of Compton collimation and yielded the best NEC.

Fig. 5 shows selected reconstructed slices through the breast of the digital phantom The randoms and trues are shown in Table 2. The maximum NEC DW algorithm reduced random coincidences by roughly 50-60% at 10-30 activity. At 30 mCi, the number of true coincidences was 11% higher than the conventional method because of the new ability to identify a fraction of trues within multiple coincidences.

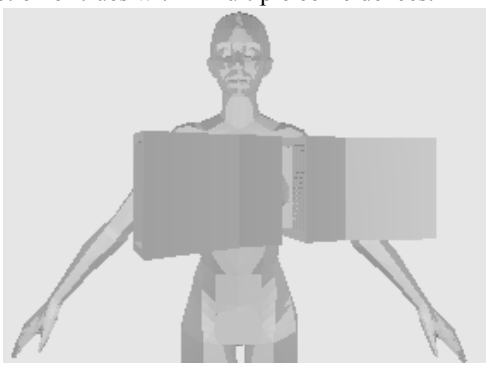

Fig. 4. Shown is an illustration of a dual-panel CZT PET system imaging one breast of a simulated human.

TABLE 1. NEC COMPARISON FOR CONVENTIONAL TIME WINDOW, OPTIMIZED FIXED THRESHOLD DIRECTION WINDOW, AND MAXIMUM NEC DW ALGORITHM.

Total activity in phantom	Conventional Time window	Optimized Fixed DW (threshold in radians)	Max. NEC DW algo.
1 mCi	1029	1036 (0.74)	1036
5 mCi	3978	4457 (0.38)	4446
10 mCi	6156	7704 (0.32)	7852
20 mCi	8663	13039 (0.25)	13313
30 mCi	9590	16931 (0.22)	17211

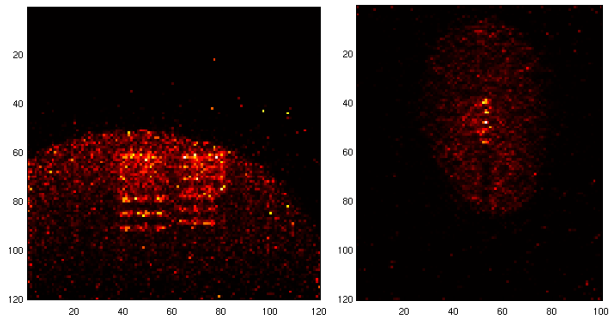

Fig. 5. Slices of a typical reconstructed image of the breast in the digital human phantom.

TABLE 2. A COMPARISON OF RANDOMS AND TRUES FOR THE STANDARD VS. MAXIMUM NEC DIRECTION WINDOW METHOD.

	Standard		Max NEC DW	
	Trues	**Randoms**	**Trues**	**Randoms**
1 mCi	1111	68	1090	38
5 mCi	5123	1396	5087	659
10 mCi	9725	5435	9913	2447
20 mCi	18525	20572	19637	8903
30 mCi	25988	43229	28852	18679

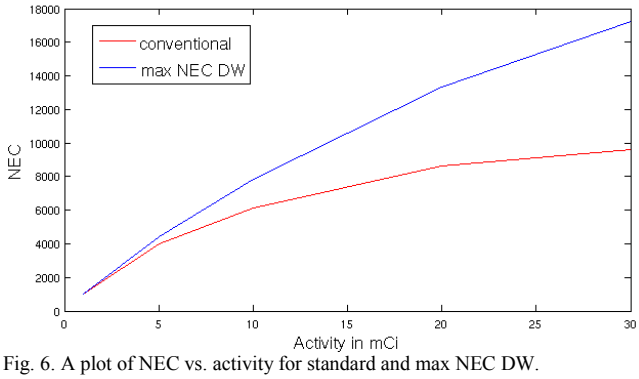

Fig. 6. A plot of NEC vs. activity for standard and max NEC DW.

The NEC vs. activity level for the standard coincidence method and the maximum NEC DW algorithm is shown in Fig. 6. At low activities, the difference between the two methods is small. As the activity increases, the maximum NEC DW algorithm achieves nearly 70% improvement to the NEC. The ~20% NEC improvement seen at 10 mCi phantom activity is considered to be clinically relevant.

VI. Discussion And Conclusion

We show that Compton collimation with 3-D detectors is possible. Furthermore, with a direction window one can filter random coincidences with minimal loss of true coincidences and recover a significant fraction of trues that were previously lost within multiples. For the simulated breast PET system, the tissue scatter fraction was less than 2%. Consequently, the effectiveness of the algorithm for filtering tissue scatter could not be assessed.

For this study, optimistic coincidence time resolution was assumed at 8 ns for CZT resulting in only a modest (up to 80% at 30 mCi) improvement to NEC. For systems with higher random coincidence rates, such as from higher activity or

worse coincidence time resolution, more significant gains in NEC are possible using the direction windowing.

ACKNOWLEDGMENT

We thank Peter D. Olcott for the use of the female phantom and breast panel models for GRAY simulations.

REFERENCES

[1] C. S. Levin, J. L. Mattesson, R. T. Skelton, M. R. Pelling, F. Duttweiler, G. Huszar, P. C. LeBlanc. "Promising characteristics and performance of cadmium zinc telluride for positron emission tomography," *2004 Nuclear Science Symposium and Medical Imaging Conference*, Rome Italy, 2004. Abstract # M2-117, Book of Abstracts, p. 136, IEEE Nuclear and Plasma Science Society.

[2] C. S. Levin, New Imaging Technologies to Enhance the Molecular Sensitivity of Positron Emission Tomography, *Proc. IEEE*, vol. 96, No. 3, pp. 439-467, 2008.

[3] Y. Okada, T. Takahashi, G. Sato, S. Watanabe, S. Nakazawa, K. Mori, and K. Makishima, "CdTe and CdZnTe detectors for timing measurements," 2001 *IEEE Nuc. Sci. Symp. Med. Imag. Conf. Rec*., no. 4, pp. 2429-2433, 2001.

[4] E. Bertolucci, M. Conti, C.A. Curto, and P. Russo, "Timing properties of CdZnTe detectors for positron emission tomography," *Nuc. Instr. Methods Phys. Res. A*, vol. 400, no. 1, pp. 107-112, 1997.

[5] L. Meng and Z. He, "Exploring the limiting timing resolution for large volume CZT detectors with waveform analysis," *Nuc. Instr. Methods A*, vol. 550, pp. 435-445, 2005.

[6] M.E. Phelps, E.J. Hoffman, N.A. Mullani, and M.M. Ter-Pogossian, "Application of annihilation coincidence detection to transaxial reconstruction tomography," *JNM*, vol. 16, no. 3, pp. 210-224, 1975.

[7] D.B. Everett, J.S. Fleming, R.W. Todd, and J.M. Nightingale, "Gamma-radiation imaging system based on the Compton effect," *Proc. IEE*, vol. 124, pp. 995-1000, 1977.

[8] M. Singh, "An electronically collimated gamma camera for single photon emission computed tomography, Part I: Theoretical considerations and design criteria," *Med. Phys.*, vol. 10, pp. 421-427, 1983.

[9] M. Singh and D. Doria, "An electronically collimated gamma camera for single photon emission computed tomography, Part II: Image reconstruction and preliminary experimental measurements," *Med. Phys.*, vol. 10, pp. 428-435, 1983.

[10] G. Chinn, A.M.K. Foudray and C.S. Levin, "A method to include single photon events in image reconstruction for a 1 mm resolution PET system built with advanced 3-D positioning detectors," *2006 IEEE Nuclear Science Symposium Conference Record*, pp. 1740-1745, 2006.

[11] S. Jan, G. Santin, D Strul, S. Staelens, K. Assié, D. Autret, S. Avner, R Barbier, M. Bardiès, PM Bloomfield, D. Brasse, V. Breton, P. Bruyndonckx, I. Buvat, A.F. Chatziioannou, Y. Choi, Y.H. Chung, C. Comtat, D. Donnarieix, L. Ferrer, S.J. Glick, C.J. Groiselle, D. Guez, P.F. Honore, S. Kerhoas-Cavata, A.S. Kirov, V. Kohli, M. Koole, M. Krieguer, D.J. van der Laan, F. Lamare, G. Largeron, C. Lartizien, D. Lazaro, M.C. Maas, L. Maigne, F. Mayet, F. Melot, C. Merheb, E. Pennacchio, J. Perez, U. Pietrzyk, F.R. Rannou, M. Rey, D.R. Schaart, C.R. Schmidtlein, L. Simon, T.Y. Song, JM. Vieira, D. Visvikis, R. Van de Walle, E. Wieërs, C. Morel, "GATE: a simulation toolkit for PET and SPECT," *Phys. Med. Biol.* vol. 49**,** 4543-4561, 2004.

[12] Y.F. Du, Z. He, G.F. Knoll, D.K. Wehe, and W. Li, "Evaluation of a Compton scattering camera using 3-D position sensitive CdZnTe detectors," *Nuc. Instr. Methods Phys. Res. A*, vol. 457, pp. 203-211, 2001.

[13] G. Pratx and C.S. Levin, "Accurately positioning events in a high-resolution PET system that uses 3D CZT detectors," *2007 IEEE Nuc. Sci. Symp Med. Imag. Conf*, pp. 2660-2664, 2007.

[14] G. Chinn, A.M.K. Foudray, and C.S. Levin, "Accurately positioning and incorporating tissue-scattered photons into PET image reconstruction," *2006 IEEE Nuclear Science Symposium Conference Record*, Vol. 3, pp. 1746-1751, Oct. 2006.

[15] G. Chinn, A.M.K. Foudray and C.S. Levin, "A method to include single photon events in image reconstruction for a 1 mm resolution PET system built with advanced 3-D positioning detectors," *2006 IEEE Nuclear Science Symposium Conference Record*, pp. 1740-1745, 2006.

[16] A. D. Whalen, *Detection of Signals in Noise*, Academic Press: San Diego, CA, 1971.

[17] S.C. Strother, M.E. Casey, and E.J. Hoffman, "Measuring PET scanner sensitivity: relating countrates to image signal-to-noise ratios using noise equivalent counts," *IEEE Trans. Nuc. Sci.*, vol. 37, no. 2, pp.783-788, 1990.

[18] P.D. Olcott, S.R. Buss, C.S. Levin, G. Pratx, C.K. Sramek, "GRAY: high energy photon ray tracer for PET applications," *2006 IEEE Nuclear Science Symposium Conference Record*, pp. 2011-2015, 2006.

[19] L.A. Shepp and Y. Vardi, "Maximum likelihood reconstruction for emission tomography," *IEEE Trans. Med. Imaging*, vol. 1., pp. 113-122, 1982.

[20] L. Parra and H.H. Barrett, "List mode likelihood: EM algorithm and image quality estimation demonstrated on 2-D PET," *IEEE Trans. Med. Imag*ing pp. 228-235, 1998.

[21] H.M. Hudson and R.S. Larkin, "Accelerated image reconstruction using ordered subsets of projected data," *IEEE Trans. Med Imaging*, vol. 13, pp. 601-609, 1994.